# *Fractal-Based Point Processes*

2005

**Steven Bradley Lowen**
*Harvard Medical School*
*McLean Hospital*

**Malvin Carl Teich**
*Boston University*
*Columbia University*

WILEY

# 7

# *Fractal Renewal Processes*

**Vilfredo Federigo Samaso Pareto (1848–1923)**, an aristocratic Italian economist associated with the University of Lausanne, discovered that scale-invariant, power-law distributions characterize the income of individuals in many societies.

Working with Jay Berger in 1963, **Benoit B. Mandelbrot (born 1924)** identified self-similar error clusters in data-transmission systems; he long ago recognized that fractals abound in many fields and set forth the principles of fractal analysis.

Perhaps the simplest fractal-based point process is the **fractal renewal process**, in which the intervals between successive events $\{\tau_n\}$ follow a decaying power-law (hyperbolic) probability density function. Like all renewal processes (see Sec. 4.2), these intervals are independent and identically distributed.

The power-law density function is known as **Pareto's Law**, in honor of Vilfredo Pareto who first established it in 1896. Pareto successfully used it to characterize a broad range of phenomena, the most celebrated of which is the income level of individuals. And, indeed, Pareto's Law has continued to enjoy widespread use in econometric and financial analyses, and in the evaluation of risk in trading (see, for example, Mandelbrot, 1960, 1964, 1982, 1997; Mandelbrot & Hudson, 2004).

A well-known modern application of this law lies in the statistics of errors following data transmission over a telephone line. In an approach promulgated by Berger & Mandelbrot (1963), a sequence of samples drawn from a power-law density forms a fractal renewal process that is used to model the occurrences of these errors. It had long been known that transmission-error occurrences appeared in clusters, and in clusters of clusters; these clusters were separated by relatively long periods of time during which no errors occurred. Using data provided by the German Federal Telephone Administration, Berger & Mandelbrot (1963) demonstrated that the intervals between errors could, in fact, be roughly described by a power-law distribution. Similar behavior also characterized the inter-error intervals between 255-bit *blocks* of data transmitted over telephone and high-frequency radio teletype circuits (Moriarty, 1963).

Mandelbrot (1965a) subsequently modified this model in a number of respects in an attempt to achieve improved agreement with the error data; he mandated self-similarity and, closely following Pareto, extended the duration of the upper interval to infinity. Indeed, Mandelbrot's (1965a) model characterized the inter-error intervals far better than the standard geometric-distribution model in use at the time (Gilbert, 1961). More recently, Mandelbrot (1972, 1982, pp. 282–284) further refined this model to make it more appealing from a mathematical perspective.

This chapter is devoted to the properties of fractal renewal point processes, which belong to the family of fractal point processes (see Sec. 5.5.1). Although less prevalent than their fractal-rate cousins, these processes find use in applications such as the characterization of computer cache misses (Voldman, Mandelbrot, Hoevel, Knight & Rosenfeld, 1983; Thiébaut, 1988) and the occurrences of earthquakes and their aftershocks (Lapenna, Macchiato & Telesca, 1998; Telesca, Cuomo, Lanfredi, Lapenna & Macchiato, 1999; Telesca, Cuomo, Lapenna & Macchiato, 2002a) (see Prob. 10.7, however). They are also useful in a number of other areas, some of which are considered in the form of problems at the end of this chapter.

## 7.1 POWER-LAW DISTRIBUTED INTEREVENT INTERVALS

With all correlations and dependencies among the intervals excluded, the fractal renewal process resets with the arrival of each event and no memory exists across events. Paradoxically, a fractal-based point process still proves possible; the scaling (fractal) behavior derives from the distribution of the intervals alone.

A probability density function that decays in a power-law form cannot conveniently persist for all values of the random variable, since the resulting probability density would have infinite area. Rather, we consider the general case in which we impose probability-density cutoffs at both small and large times, as shown in Fig. 7.1. This ensures that the resulting point process has a positive rate in the stationary (equilibrium) state.

### 7.1.1 Abrupt-cutoff interevent-interval density

The abrupt-cutoff power-law probability density function provides the simplest example (Lowen & Teich, 1993d):

$$p_\tau(t) = \frac{\gamma}{A^{-\gamma} - B^{-\gamma}} \times \begin{cases} t^{-(\gamma+1)} & A < t < B \\ 0 & \text{otherwise,} \end{cases} \tag{7.1}$$

where $B > A > 0$ and $\gamma > 0$. The associated moments are

$$\mathrm{E}[\tau^n] = \begin{cases} \dfrac{\gamma}{n-\gamma}\,(A/B)^\gamma\, B^n \dfrac{1-(A/B)^{n-\gamma}}{1-(A/B)^\gamma} & n \neq \gamma \\ \dfrac{\gamma \ln(B/A)}{A^{-\gamma} - B^{-\gamma}} & n = \gamma, \end{cases} \tag{7.2}$$

while the characteristic function is

$$\phi_\tau(\omega) = \frac{\gamma\,(i\omega)^\gamma}{A^{-\gamma} - B^{-\gamma}} \int_{i\omega A}^{i\omega B} e^{-x}\, x^{-(\gamma+1)}\, dx. \tag{7.3}$$

The **Pareto density** (1896) emerges in the special case $A = 1$ and $B \to \infty$. For $A \ll B$ and $0 < \gamma < 1$, we can express Eq. (7.3) as (Lowen, 1992)

$$1 - \phi_\tau(\omega) \approx \Gamma(1-\gamma)\,(i\omega A)^\gamma \tag{7.4}$$

in the range $B^{-1} \ll \omega \ll A^{-1}$.

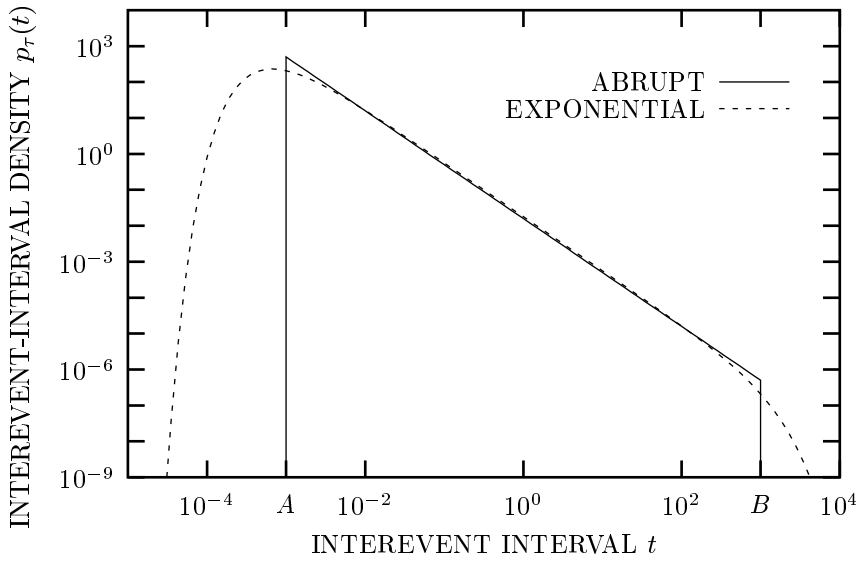


***Fig. 7.1*** Abrupt-cutoff (solid) and exponential-cutoff (dashed) interevent-interval probability density functions, $p_\tau(t)$ vs. $t$. The density functions exhibit a power-law region between $t = A$ and $t = B$. In this illustration, we set the lower and upper cutoffs at $A = 10^{-3}$ and $B = 10^3$, respectively. The power-law exponent of the density has a value $-\frac{3}{2} = -(\gamma + 1)$ so that $\gamma = \frac{1}{2}$.

### 7.1.2 Exponential-cutoff interevent-interval density

We can impose smooth transitions on this power-law behavior by using the interevent-interval density function (Lowen & Teich, 1993d)

$$p_\tau(t) = \frac{(AB)^{\gamma/2}}{2\mathrm{K}_\gamma\Big(2\sqrt{A/B}\Big)}\, e^{-A/t}\, e^{-t/B}\, t^{-(\gamma+1)}, \tag{7.5}$$

where $\mathrm{K}_\gamma(x)$ denotes the modified Bessel function of the second kind of order $\gamma$. It is sometimes referred to as the **generalized inverse Gaussian density** (Barndorff-Nielsen, Blaesild & Halgreen, 1978).

The associated moments then become

$$\mathrm{E}[\tau^n] = (AB)^{n/2}\, \frac{\mathrm{K}_{|\gamma-n|}\Big(2\sqrt{A/B}\Big)}{\mathrm{K}_\gamma\Big(2\sqrt{A/B}\Big)}, \tag{7.6}$$

and the corresponding characteristic function can be written as

$$\phi_\tau(\omega) = (1 + i\omega B)^{\gamma/2}\, \frac{\mathrm{K}_\gamma\big[2(A/B + i\omega A)^{1/2}\big]}{\mathrm{K}_\gamma\Big(2\sqrt{A/B}\Big)}. \tag{7.7}$$

For $\gamma = \frac{1}{2}$ and $B \to \infty$, Eq. (7.7) becomes the one-sided **stable distribution** of order $\frac{1}{2}$ (Feller, 1971), which was provided previously in Eq. (3.13). Combined with exponential tails, one-sided stable distributions for arbitrary values of $\gamma$ between zero and unity also follow power-law forms while providing smooth transitions (Lowen, 1992).

Constructing a renewal point process using any of these random variables leads to a point process with fractal properties, as we will demonstrate shortly.

### 7.1.3 Effect of $\gamma$ on interval variability

Whatever the nature of the cutoff, as $B \to \infty$ the character of the process changes as $\gamma$ passes through unity. Values of $\gamma$ smaller than unity lead to intervals with infinite mean, whereas values of $\gamma$ in excess of two ensure finite variance. In the range $1 < \gamma < 2$, the interevent intervals have finite mean but exhibit wild variation about that mean as a result of the infinite variance of the intervals in this range. As a general rule of thumb, the variability decreases as $\gamma$ increases.

When $B$ is finite, so that all moments are finite, the value of $\gamma$ nevertheless continues to play an important role in determining the variability of the intervals. As $\gamma$ increases, the interval density becomes more concentrated near the lower cutoff, $A$, with proportionately fewer intervals near $B$. This results in a renewal process with reduced variability. Equation (7.2) highlights this effect; the mean interevent interval in the limit $A/B \ll 1$ is $\mathrm{E}[\tau] \approx \sqrt{AB}$ for $\gamma = \frac{1}{2}$ whereas it is $\mathrm{E}[\tau] \approx 3A$ for $\gamma = \frac{3}{2}$. Since $\mathrm{E}[\tau]$ is independent of $B$ for $\gamma > 1$ and $A/B \ll 1$, relatively few intervals lie near $B$. Extreme events are therefore relatively less likely than for $\gamma < 1$.

## 7.2 STATISTICS OF THE FRACTAL RENEWAL PROCESS

### 7.2.1 Point-process spectrum

We begin with the point-process spectrum of the fractal renewal point process. In the mid-frequency range, $B^{-1} \ll f \ll A^{-1}$, we obtain (see Sec. A.4.1 and Lowen, 1992; Lowen & Teich, 1993d):

$$S_N(f) \to \mathrm{E}[\mu] \times \begin{cases} 2\left[\Gamma(1-\gamma)\right]^{-1} \cos(\pi\gamma/2)\,(2\pi f A)^{-\gamma} & 0 < \gamma < 1 \\ \pi\left[\ln(2\pi f A)\right]^{-2}\,(2\pi f A)^{-1} & \gamma = 1 \\ 2\gamma^{-2}\,(\gamma-1)\,\Gamma(2-\gamma)\left[-\cos(\pi\gamma/2)\right]\,(2\pi f A)^{\gamma-2} & 1 < \gamma < 2 \\ -\frac{1}{2}\ln(2\pi f A) & \gamma = 2 \\ \gamma^{-1}\,(\gamma-2)^{-1} & \gamma > 2. \end{cases} \tag{7.8}$$

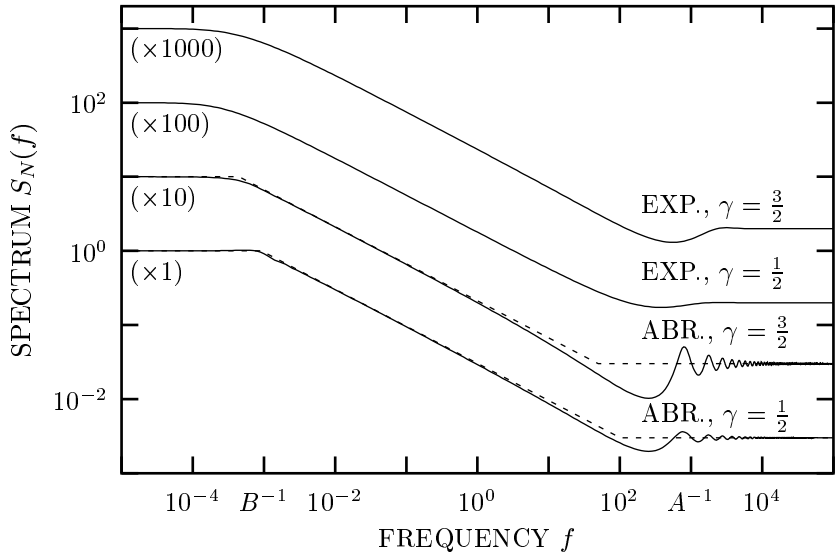


***Fig. 7.2*** Normalized spectra, $S_N(f)\,/\lim_{f\to 0} S_N(f)$, for the fractal renewal point process. In this illustration, $A = 10^{-3}$ and $B = 10^3$. The four solid curves represent spectra corresponding to different interevent-interval densities, with the following properties (top to bottom): exponential cutoffs with $\gamma = \frac{3}{2}$ ($\times 1\,000$), exponential cutoffs with $\gamma = \frac{1}{2}$ ($\times 100$), abrupt cutoffs with $\gamma = \frac{3}{2}$ ($\times 10$), and abrupt cutoffs with $\gamma = \frac{1}{2}$ ($\times 1$). The curves were obtained by using Eqs. (7.3) and (7.7) in Eq. (4.16), for the abrupt and exponential cutoffs, respectively. The dashed curves are asymptotic forms for the abrupt-cutoff interevent-interval densities, drawn from the low-, mid-, and high-frequency spectral limits represented by Eqs. (4.17), (7.8), and (3.59), respectively. All four spectra decrease with frequency as $f^{-1/2}$ in the region $B^{-1} \ll f \ll A^{-1}$, in accordance with Eq. (7.9); however, those for $\gamma = \frac{3}{2}$ depart more markedly from the asymptotic values than do those for $\gamma = \frac{1}{2}$. Spectra associated with abrupt-cutoff interval probability densities exhibit marked oscillations at higher frequencies.

Equation (7.8) reveals that the value of $\alpha$ associated with the spectrum depends on $\gamma$ in accordance with

$$\alpha = \begin{cases} \gamma & 0 < \gamma < 1 \\ 2 - \gamma & 1 < \gamma < 2 \\ 0 & \gamma > 2. \end{cases} \tag{7.9}$$

Thus, $\alpha$ neither attains, nor exceeds, unity over the mid-frequency range. Indeed, this kind of behavior emerges for all power-law forms of the interevent-interval density; hence the fractal renewal point process generates $1/f^\alpha$ noise only in the range $0 < \alpha < 1$.

Figure 7.2 displays the spectra for abrupt and exponential cutoffs, normalized to the values indicated at the low-frequency limits. We generated these curves by making use of Eq. (4.16), together with Eqs. (7.3) and (7.7) for the abrupt and exponential cutoffs, respectively. The low-, mid-, and high-frequency asymptotes are set forth in

Eqs. (4.17), (7.8), and (3.59), respectively. The abrupt-cutoff probability density functions exhibit substantial oscillations in the characteristic function, which appear in the spectra. The exponential-cutoff density functions, in contrast, generate smooth transitions in the time domain and therefore nonoscillatory spectra. Interevent-interval probability density functions with $\gamma = \frac{1}{2}$ and $\gamma = \frac{3}{2}$ both translate to spectra that exhibit a fractal spectral exponent $-\alpha = -\frac{1}{2}$, but the latter depart more markedly from asymptotic values. A simulated version of the spectrum for the abrupt-cutoff case with $\gamma = \frac{3}{2}$ is shown in Fig. B.12.

We can derive a closed-form expression for the spectrum for the smooth-transition interevent-interval probability density function given in Eq. (7.5) for $\gamma = \frac{1}{2}$; we consider the normalized case $AB = 1$ to simplify the ensuing calculations (see Sec. A.4.2):

$$S_N(f) = \mathrm{E}^2[\mu]\,\delta(f) + \frac{\sinh(c)}{\cosh(c) - \cos(d)}, \tag{7.10}$$

with

$$c \equiv \sqrt{2A}\left(\sqrt{A^2+\omega^2} + A\right)^{1/2} - 2A \tag{7.11}$$

$$d \equiv \sqrt{2A}\left(\sqrt{A^2+\omega^2} - A\right)^{1/2}. \tag{7.12}$$

In fact, given enough patience, closed-form expressions can be derived for $\gamma = n + \frac{1}{2}$, where $n$ is any nonnegative integer.

### 7.2.2 Coincidence rate

Inverse Fourier transforms of the abrupt-cutoff spectrum formulas given in Eq. (7.8) are readily calculated. This leads to approximate formulas for the coincidence rate of the power-law process in the range $A \ll |t| \ll B$, for positive values of $\gamma$ (see Sec. A.4.3):

$$G(t) \to \mathrm{E}[\mu] \times \begin{cases} \pi^{-1}\sin(\pi\gamma)\,A^{-\gamma}\,t^{\gamma-1} & 0 < \gamma < 1 \\ A^{-1}\left[\ln(t/A)\right]^{-1} & \gamma = 1 \\ \gamma^{-2}\,(\gamma-1)\,A^{\gamma-2}\,t^{1-\gamma} & 1 < \gamma < 2 \\ \frac{1}{4}\,t^{-1} & \gamma = 2 \\ \mathrm{E}[\mu] & \gamma > 2. \end{cases} \tag{7.13}$$

For the exponential-cutoff interevent-interval density provided in Eq. (7.5) and $\gamma = \frac{1}{2}$, we can write the coincidence rate in the following form:

$$\begin{aligned} G(t) &= \mathrm{E}[\mu]\,\delta(t) + \mathrm{E}[\mu]\sum_{n=1}^{\infty} p^{\star n}(|t|) \\ &= (AB)^{-1/2}\,\delta(t) + (\pi B)^{-1/2}\,|t|^{-3/2}\,\exp(-|t|/B) \\ &\quad \times \sum_{n=1}^{\infty} n\exp\left[2(A/B)^{1/2}\,n - (A/|t|)\,n^2\right]. \end{aligned} \tag{7.14}$$

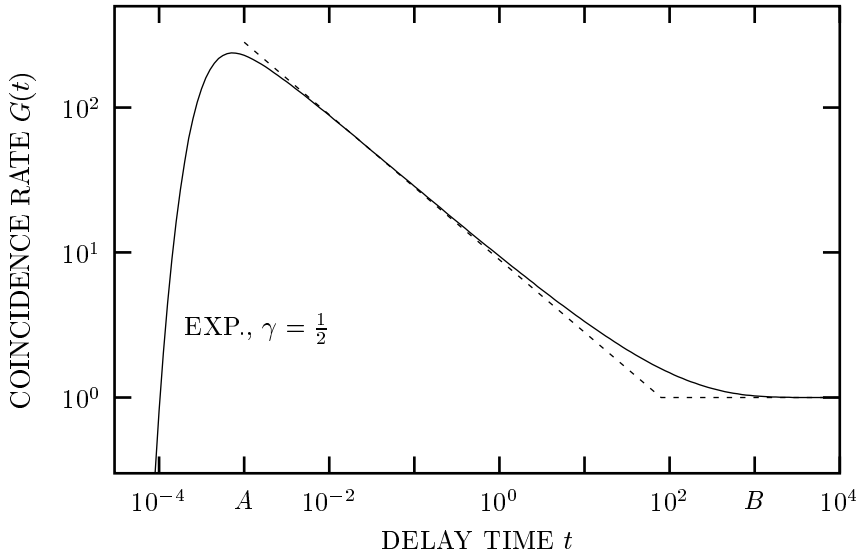


***Fig. 7.3*** Coincidence rate for a fractal renewal point process constructed with the exponential-cutoff probability density function specified in Eq. (7.5). The parameters are $\gamma = \frac{1}{2}$, $A = 10^{-3}$, and $B = 10^3$ (solid curve). The straight-line asymptotes derive from simplifying Eq. (7.15) in the limit $|t| \ll B$ and from Eq. (3.51).

In the limit $|t| \gg A$ and $B \gg A$, the terms comprising the sum in Eq. (7.14) vary slowly. An integral then provides a good approximation to the sum, and the coincidence rate simplifies to

$$\begin{aligned} G(t) &\approx (\pi B)^{-1/2} \, |t|^{-3/2} \, e^{-|t|/B} \int_0^\infty x \, \exp\left[2(A/B)^{1/2} \, x - (A/|t|) \, x^2\right] dx \\ &= \frac{e^{-|t|/B}}{\sqrt{4\pi A^2 B \, |t|}} + \frac{1}{2AB} \, \mathrm{erfc}\left(-\sqrt{\frac{|t|}{B}}\right), \end{aligned} \tag{7.15}$$

where the complementary error function is given by

$$\mathrm{erfc}(x) \equiv 2\pi^{-1/2} \int_x^\infty \exp(-t^2) \, dt. \tag{7.16}$$

The coincidence rate represented in Eqs. (7.14)–(7.16), which is applicable for exponential cutoffs and $\gamma = \frac{1}{2}$, is displayed in Fig. 7.3.

### 7.2.3 Normalized variances

The counting statistics of renewal point processes are often provided in terms of a special type of factorial moment, set forth in Eq. (4.19). For the fractal renewal point

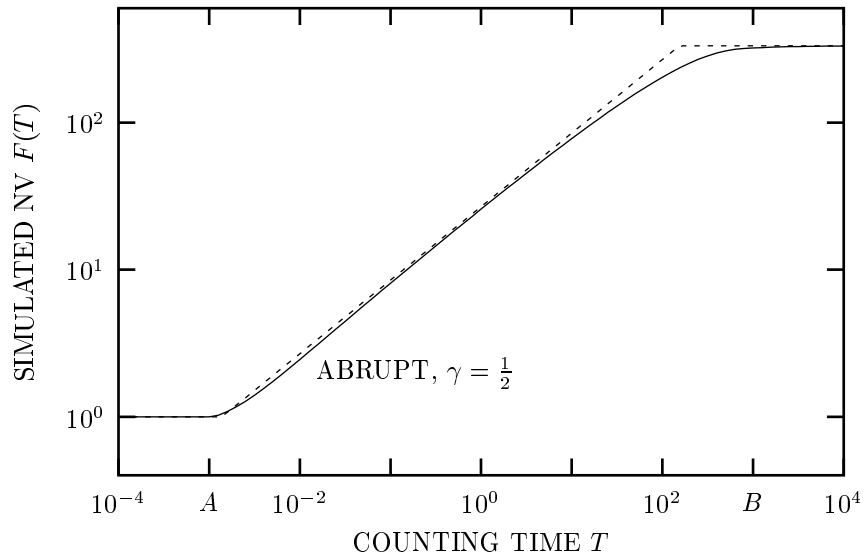


***Fig. 7.4*** Simulated normalized variance $F(T)$ vs. counting time $T$ for a fractal renewal point process with abrupt cutoffs (solid curve). The parameters used to generate this curve are $\gamma = \frac{1}{2}$ ($\alpha = \frac{1}{2}$), $A = 10^{-3}$, and $B = 10^3$; 100 independent simulations were used, each of duration $L = 10^8$. Asymptotic results are shown as dashed. The mean rate is unity ($\mathrm{E}[\mu] = \mathrm{E}[\tau] = 1$). The associated normalized Haar-wavelet variance is shown in Fig. 7.5.

process at hand, we can cast these factorial moments in relatively simple form when $A \ll |t| \ll B$ and $0 < \gamma < 1$, even for arbitrary cutoffs.

Since $G(t) \sim t^{\gamma-1}$, we have $G^{\star k}(t) \sim t^{k\gamma-1}$, whereupon Eq. (4.19) provides

$$\mathrm{E}\left\{\frac{[Z(T)+k]!}{[Z(T)-1]!}\right\} \sim T^{k\gamma+1}. \tag{7.17}$$

The constants of proportionality depend on the details of the interevent-interval probability density function.

In particular, for the abrupt-cutoff fractal renewal point process with arbitrary $\gamma$, we can readily obtain expressions for the normalized variance and normalized Haar-wavelet variance in the range $A \ll T \ll B$. Substituting Eq. (7.13) into Eqs. (3.52) and (3.53) yields $F(T)$ and $A(T)$, respectively (see Sec. A.4.4):

$$F(T) \to \begin{cases} 2\big[\pi\gamma(\gamma+1)\big]^{-1} \sin(\pi\gamma)\, A^{-\gamma}\, T^{\gamma} & 0 < \gamma < 1 \\ A^{-1}\big[\ln(T/A)\big]^{-1}\, T & \gamma = 1 \\ 2\big[\gamma^2(2-\gamma)(3-\gamma)\big]^{-1}\, (\gamma-1)\, A^{\gamma-2}\, T^{2-\gamma} & 1 < \gamma < 2 \\ \frac{1}{2}\ln(T/A) & \gamma = 2 \\ 1 & \gamma > 2 \end{cases} \tag{7.18}$$

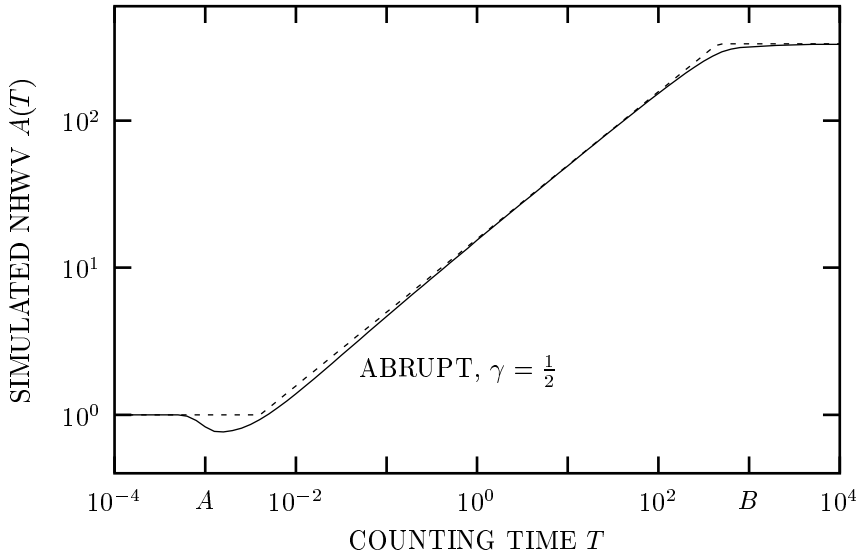


***Fig. 7.5*** Simulated normalized Haar-wavelet variance $A(T)$ vs. counting time $T$ for a fractal renewal point process with abrupt cutoffs (solid curve). The parameters are the same as those specified in Fig. 7.4, which displays the associated normalized variance. We show asymptotic results as dashed lines. A simulated version of $A(T)$ for $\gamma = \frac{3}{2}$, which also corresponds to $\alpha = \frac{1}{2}$, appears in Fig. B.13. The dip in the curve derives from the abrupt cutoff in the interevent-interval density for small intervals.

while

$$A(T) \to \begin{cases} 4(1-2^{\gamma-1})\left[\pi\gamma(\gamma+1)\right]^{-1}\sin(\pi\gamma)\,A^{-\gamma}\,T^{\gamma} & 0<\gamma<1 \\ 2\ln(2)\,A^{-1}\left[\ln(T/A)\right]^{-2}T & \gamma=1 \\ 4(1-2^{1-\gamma})\left[\gamma^2(2-\gamma)(3-\gamma)\right]^{-1}(\gamma-1)\,A^{\gamma-2}\,T^{2-\gamma} & 1<\gamma<2 \\ \frac{1}{2}\ln(T/2A) & \gamma=2 \\ 1 & \gamma>2. \end{cases} \tag{7.19}$$

Since it is difficult to obtain useful analytic forms for the normalized variance $F(T)$ and the normalized Haar-wavelet variance $A(T)$ over the full range of counting times $T$, we present simulations for these quantities as functions of $T$ in Figs. 7.4 and 7.5, respectively. The solid curves represent simulated results for $\gamma = \frac{1}{2}$ ($\alpha = \frac{1}{2}$); the central asymptotes (dashed lines) represent Eqs. (7.18) and (7.19), respectively. A cartoon version of the normalized Haar-wavelet variance was presented earlier, as the solid curve in Fig. 5.4d).

### 7.2.4 Counting distribution

We present simulated counting distributions in Fig. 7.6 for $\gamma = \frac{1}{2}$ (solid curve) and $\gamma = \frac{3}{2}$ (dashed curve), when the mean count $\mathrm{E}[Z] = 10$. Again, we employ simulations because tractable analytic results cannot be obtained. We display the curves on doubly logarithmic coordinates to highlight the different count ranges spanned by the two curves. Although the *interevent-interval* standard deviations are identical for the two values of $\gamma$, the variances of the associated *counting* distributions are very different. Estimating these values from the simulated counting distributions yields $\mathrm{Var}[Z(10\,\mathrm{E}[\tau])] \doteq 777.703$ for $\gamma = \frac{1}{2}$ and $\mathrm{Var}[Z(10\,\mathrm{E}[\tau])] \doteq 28.9254$ for $\gamma = \frac{3}{2}$. As expected, the variance is larger for the smaller value of $\gamma$. We also plot a Poisson distribution of the same mean for comparison (dotted curve). These fractal-renewal-process counting distributions are distinctly non-Gaussian. However, the renewal nature of the process and the finite cutoffs assure us that they converge to Gaussian form for $T/B \gg 1$; Eq. (4.18) applies in that domain. Identical counting distributions obtain when $A$, $B$, and $T$ are all multiplied by a common factor, since the determining parameters are *ratios* between the times rather than the times themselves.

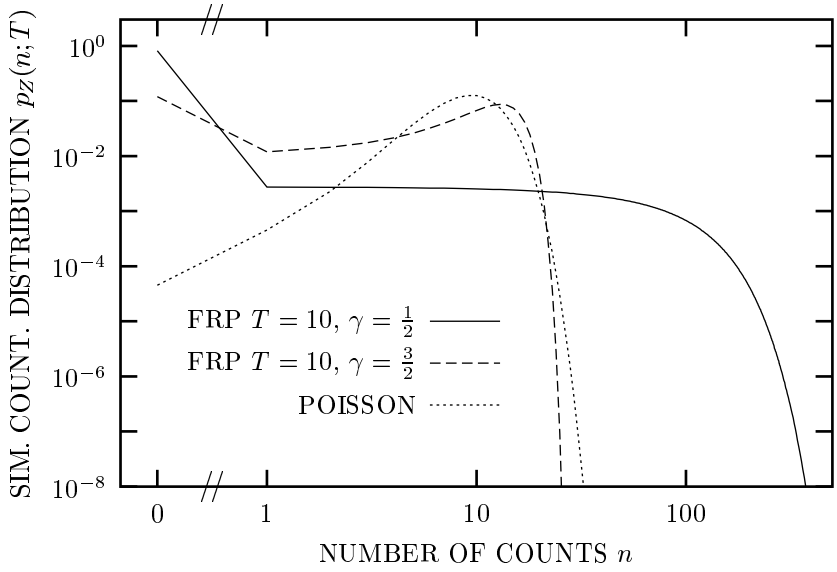


***Fig. 7.6*** Simulated counting distributions, $p_Z(n;T)$ vs. number of counts $n$, for two fractal renewal point processes with abrupt cutoffs. The parameters used to generate these curves were $\mathrm{E}[\tau] = 1$, $T = 10$, and $B/A = 10^6$. These values, in turn, give rise to the following exact (not rounded) values for the remaining parameters. For $\gamma = \frac{1}{2}$ we have: $A = 10^{-3}$, $B = 10^3$, and $\mathrm{Var}[\tau] = 332.667$; for $\gamma = \frac{3}{2}$ we have: $A = 0.333667$, $B = 333667.0$, and again $\mathrm{Var}[\tau] = 332.667$.

### 7.2.5 Capacity dimension

Calculation of the capacity dimension (see Secs. 2.1.1 and 3.5.4) yields the expected result: for the parameter ranges $0 < \gamma < 1$ and $0 < A \ll B < \infty$, the points generated by the fractal renewal process do indeed form a fractal set with dimension $\gamma$, in the sense of Eq. (3.72) (Lowen & Teich, 1993d).

Consider a realization of the process and a covering of it using segments of length $\mathcal{B}$, as shown in Fig. 7.7. For minimal covering, place the beginning of each segment on the first uncovered event. The empty space between coverings is thus the residual waiting time for a pure renewal point process at time $\mathcal{B}$. This construction closely resembles that for fixed dead time, which is illustrated in Fig. 11.1d) and discussed in Sec. 11.2.4.

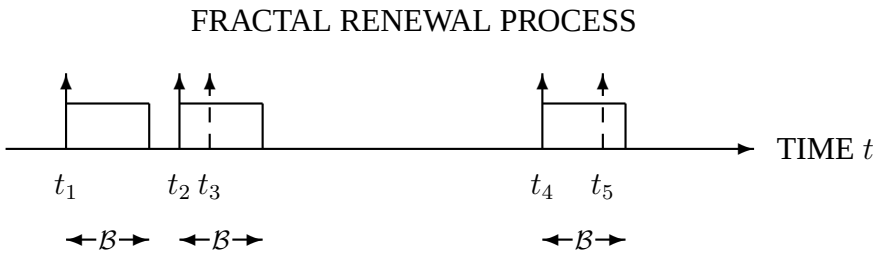


***Fig. 7.7*** Realization of a fractal renewal point process and its minimal covering. For this particular illustration, three segments suffice to cover the set. Events occurring at $t_3$ and $t_5$ lie within a duration $\mathcal{B}$ of the prior event at which a segment initiates, and therefore do not require additional segments.

Let $W(\mathcal{B})$ represent the expected value of the time between coverings, including the coverings themselves. Wald's Lemma (Feller, 1971) then provides

$$W(\mathcal{B}) = \mathrm{E}^2[\tau] \int_{0-}^{\mathcal{B}} G(t)\, dt, \tag{7.20}$$

where the notation $0-$ indicates that the range of the integral spans the delta function contribution to $G(t)$ at $t = 0$. For the range $A \ll \mathcal{B} \ll B$, the approximation $G(t) \sim t^{\gamma-1}$ yields $W(\mathcal{B}) \sim \mathcal{B}^{\gamma}$. The number of intervals required to cover the fractal renewal point process thus scales as $\mathcal{B}^{-\gamma}$, and the capacity dimension is therefore $\gamma$.

## 7.3 NONDEGENERATE REALIZATION OF A ZERO-RATE PROCESS

Both versions of the fractal renewal point process set forth in Sec. 7.1, namely the abrupt- and exponential-cutoff forms, can be extended to $B \to \infty$. The associated interevent-interval probability density functions then become

$$p_\tau(t) = \begin{cases} \gamma A^\gamma\, t^{-(\gamma+1)} & t > A \\ 0 & t \le A, \end{cases} \tag{7.21}$$

and

$$p_\tau(t) = \frac{1}{\Gamma(\gamma)}\, A^\gamma\, e^{-A/t}\, t^{-(\gamma+1)}, \tag{7.22}$$

respectively. Equation (7.21) is often called the **generalized Pareto density**.

Focusing on the case $0 < \gamma < 1$, both interevent-interval probability density functions are well defined; however, the moments of $\tau$, $\mathrm{E}[\tau^n]$, are infinite for all positive integers $n$. In particular, $\mathrm{E}[\tau] = \infty$, so that $\mathrm{E}[\mu] = 1/\mathrm{E}[\tau] = 0$, indicating that the resulting renewal point process has zero rate in the stationary (equilibrium) case. Since the rate cannot assume negative values, this implies, with probability one, that no events can occur in any finite interval.

However, we can extend the framework considered earlier for the positive-rate stationary fractal renewal point process and, in fact, obtain nontrivial results for the zero-rate nonstationary case. For renewal point processes that are not in equilibrium, but rather begin with an event, the zero-rate argument does not apply and the resulting statistics can indeed assume nondegenerate values. A segment of such a nonstationary renewal point processes can therefore contain a positive number of events, even though the mean number of events in a comparable segment of the stationary process assumes a value of zero. For the interevent-interval probability density functions specified in Eqs. (7.21) and (7.22), the probability of observing zero events in a segment of length $T$ can still become vanishingly small as the ratio $T/A$ increases.

In general, a fractal renewal point process that begins with the occurrence of an event, with an associated interevent-interval probability density function $p(t) \sim t^{-(\gamma+1)}$, has a residual waiting time that approaches a limiting density (Feller, 1971). Specifically, suppose that we can cast the interevent-interval survivor function in the form

$$\mathsf{S}_\tau(t) = 1 - P_\tau(t) = \int_t^\infty p(v)\, dv = t^{-\gamma} L(t), \tag{7.23}$$

where $L(t)$ is a "slowly varying" function such that, for any $x > 0$,

$$\lim_{t\to\infty} L(xt)/L(t) = 1. \tag{7.24}$$

Equations (7.21) and (7.22) both fall in this category. Recall, now, from Eq. (3.10) that $\vartheta(t)$ denotes the random interval between the deterministic time $t$ and the next event in the fractal renewal point process. This random interval $\vartheta(t)$ then has a probability density function given by (Feller, 1971)

$$p_\vartheta(s) = \frac{t^\gamma \sin(\pi\gamma)}{\pi}\, \frac{s^{-\gamma}}{s+t}. \tag{7.25}$$

Thus, when a fractal renewal point process with zero mean rate begins at the occurrence of an event, the resulting process has a nonzero effective rate for all finite times. We conclude that any experiment will, of necessity, record a process with a positive expected rate, and the results derived above will also apply to this process.

Any realization of an infinite-mean fractal renewal point process that begins with an event, and which we observe for a finite time, will exhibit largest and smallest intervals, which we label $B^*$ and $A^*$, respectively. Given the power-law exponent

of the distribution, and only the values $A^*$ and $B^*$, the other intervals will follow a power-law distribution between them, and will exhibit the same power-law exponent. The observed process will therefore have the same statistics as a finite-mean fractal renewal point process, with cutoff times $A < A^*$ and $B > B^*$, and the results derived above will apply to this process with the *a posteriori* values of $A^*$ and $B^*$. Although we cannot know the values $A^*$ and $B^*$ *a priori*, the sample spectrum will decay in a power-law fashion, whatever these values may be.

### *Problems*

**7.1** *Distinct processes with a common fractal exponent* Use the abrupt-cutoff power-law probability density function provided in Eq. (7.1) to construct two different fractal renewal point processes that have the following parameters: fractal exponent $\alpha = \frac{1}{2}$, fractal onset frequency $f_S = 10$ Hz, and $B/A = 10^6$. Find the mean rate $\mathrm{E}[\mu]$ for both.

**7.2** *Characteristic function for the exponential-cutoff interval density* Find an approximate expression for the characteristic function along the lines of Eq. (7.4), but for the smoother interevent-interval density function provided in Eq. (7.5). Note that the modified Bessel function of the second kind varies as $\mathrm{K}_\gamma(z) \approx 2^{\gamma-1}\,\Gamma(\gamma) z^{-\gamma}$ for small arguments $z$ (Gradshteyn & Ryzhik, 1994, Secs. 8.445 and 8.485).

**7.3** *Deriving the point-process spectrum from the characteristic function* Use Eq. (7.4) to reproduce the $0 < \gamma < 1$ condition in Eq. (7.8).

**7.4** *Relation of mean rate and fractal onset frequency* Consider the abrupt-cutoff power-law density in Eq. (7.1) for $A \ll B$.

**7.4.1.** Find an equation that relates the mean rate $\mathrm{E}[\mu]$ to the fractal onset frequency $f_S$ in the range $1 < \gamma < 2$.

**7.4.2.** Find an inequality that relates these quantities in the range $0 < \gamma < 1$.

**7.5** *Limiting form for the characteristic function* Show that Eq. (7.4) obtains for the stated limits.

**7.6** *Simulation time* To obtain good estimates of $F(T)$ and $A(T)$ for presentation in Figs. 7.4 and 7.5, we made use of 100 independent simulations of fractal renewal point processes, each of duration $10^8$. The simulation of the point processes and the calculation of these statistics took about 24 hours of computation time on a personal computer with a clock speed of 1.6 GHz. The simulated point processes were represented by floating-point numbers at four bytes per interevent interval; for fastest execution times these numbers were stored in memory for the calculation of $F(T)$ and $A(T)$. Why were curves for $\gamma = \frac{3}{2}$ with the same values for $A$ and $B$ not included in these figures?

**7.7** *Error clustering in telephone networks* In the 1960s, researchers began to recognize that data errors following information transmission over telephone lines could not be properly described by a memoryless binary symmetric channel, with its attendant geometric distribution of inter-error intervals and binomial distribution of

error counts. Gilbert (1961) attempted to improve the state of affairs by considering a channel that switched between two states that suffered different error probabilities. This added variability allowed some qualitative features of the data to be modeled, but this approach fell far short of providing detailed agreement.

Shortly thereafter, Berger & Mandelbrot (1963) and Mandelbrot (1965a) made a substantial advance. These authors recognized that a fractal renewal point process, with power-law rather than geometric inter-error intervals, provided a far superior model for characterizing the data errors. It had long been known that such errors appeared to occur in clusters, and in clusters of clusters, a feature that is the hallmark of a fractal point process.

Consider a system that exhibits errors that obey this fractal-renewal-process model. Suppose now that we add another source of noise, independent of the first, that takes the form of a homogeneous Poisson process with a large mean time between events $\tau_{\mathrm{HPP}}$. The overall noise process then comprises the superposition of error events, which are clustered, and events associated with the homogeneous Poisson process, which are not clustered. If the presence (or absence) of an error cluster is verified every $\tau_{\mathrm{clk}}$ seconds, determine the process that characterizes the error events.

**7.8** *Action-potential statistics in an insect visual-system interneuron: Counter-example* The curve in Fig. 7.8 displays the estimated interevent-interval density

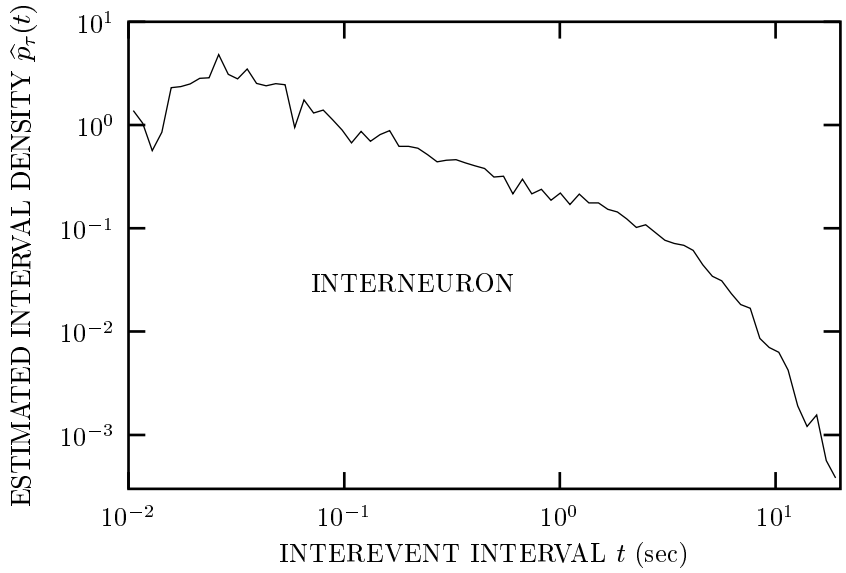


***Fig. 7.8*** Estimated interevent-interval density, $\widehat{p}_\tau(t)$ vs. interevent interval $t$, for an action-potential sequence recorded from the descending contralateral movement detector, a visual-system INTERNEURON in the locust (Turcott et al., 1995, Fig. 2, pp. 261–262, cell ADA062). The normalized Haar-wavelet variance for these same data appears in Fig. 7.9.

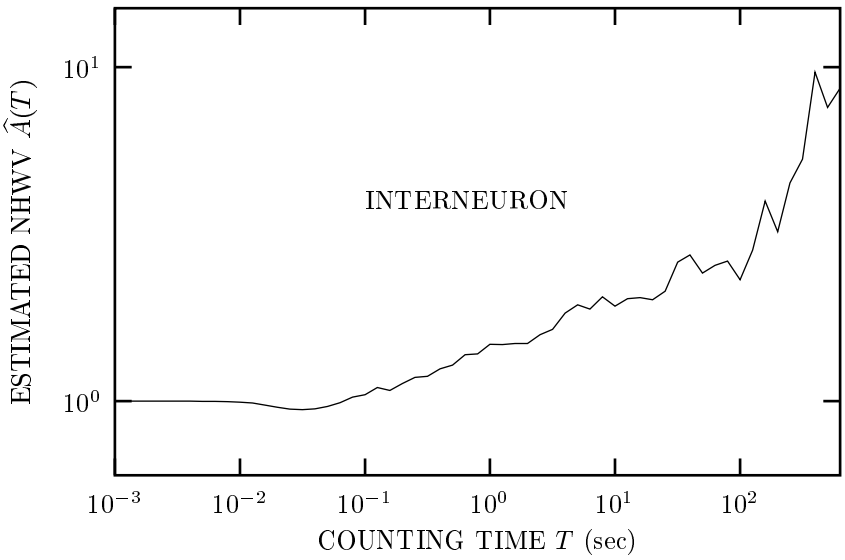


***Fig. 7.9*** Estimated normalized Haar-wavelet variance $\widehat{A}(T)$ vs. counting time $T$ (sec), for an action-potential sequence recorded from the descending contralateral movement detector, a visual-system INTERNEURON in the locust (Turcott et al., 1995, Fig. 2, pp. 261–262, cell ADA062). Unlike the display provided in Fig. 5.2, the abscissa reports the counting time in unnormalized form. The interevent-interval density for these same data appears in Fig. 7.8.

function for a spontaneous sequence of action potentials recorded from a visual-system INTERNEURON in the locust, the descending contralateral movement detector (Turcott et al., 1995), plotted on doubly logarithmic coordinates. The curve in Fig. 7.9 shows the estimated normalized Haar-wavelet variance $\widehat{A}(T)$, plotted as a function of the counting time $T$, for these same data.

**7.8.1.** Determine the values of $\widehat{\gamma}$, $\widehat{A}$, and $\widehat{B}$ that characterize the interval data in Fig. 7.8. What is the corresponding value of $\widehat{\alpha}$ for a fractal renewal point process?

**7.8.2.** What is the origin of the slight dip below unity observed in the data in Fig. 7.9? Determine the values of $\widehat{\alpha}_A$ and $\widehat{T}_A$ that characterize this plot.

**7.8.3.** Why does the value of $\widehat{\alpha}_A$ observed from the normalized Haar-wavelet variance differ so drastically from the value predicted for a fractal renewal point process?

**7.9** *Molecular evolution* The numbers of differences in amino-acid sequences in related organisms appear to be roughly proportional to the time since the organisms diverged in their joint evolutionary history (Zuckerkandl & Pauling, 1962). This leads to the notion of a molecular clock (Zuckerkandl & Pauling, 1965). While this process lacks extensive data, the existing data are adequate to exclude the homogeneous Poisson process as a viable model (Gillespie, 1994). Review the evidence presented by Gillespie (1994); West & Bickel (1998); Bickel & West (1998a,b); and Bickel

(2000), and provide a rationale for the use of a fractal renewal point process to model the available data.

**7.10** *Trapping in amorphous semiconductors* A number of approaches have been used to investigate the relationship between trapping processes and $1/f$ noise in semiconductors (McWhorter, 1957; Stepanescu, 1974; Scher & Montroll, 1975; Tiedje & Rose, 1980; Orenstein, Kastner & Vaninov, 1982; Kastner, 1985; Hooge, 1995, 1997). In particular, the multiple trapping model forges a connection between traps that are exponentially distributed over a large range of energies and a transient current that decays as a power-law function of time. Once emitted by a trap, a carrier is available to conduct current for a very brief interval of time before it falls into another trap. For any particular carrier, the times spent in successive traps are independent. Consider an amorphous semiconductor with localized states (traps) whose energies are exponentially distributed, with parameter $E_0$, between the limits $E_L$ and $E_H$. If the random variable $E$ represents the trap energy relative to the conduction band edge, the probability density function for the trap energy $p_E(E)$ is

$$p_E(E) = \begin{cases} c \exp(-E/E_0) & E_L < E < E_H \\ 0 & \text{otherwise,} \end{cases} \tag{7.26}$$

where $c$ is a normalization constant.

**7.10.1.** Determine the value of $c$ in terms of the remaining parameters of the model.

**7.10.2.** For a trap at energy $E$, the corresponding mean waiting time $q(E) = \mathrm{E}[\tau]$ is given by $\tau_0 \exp(E/\kappa\mathcal{T})$, where $\tau_0$ is the average vibrational period of the atoms in the semiconductor, $\kappa$ is Boltzmann's constant, and $\mathcal{T}$ is the absolute temperature of the material. Show how to recast the multiple trapping model for a single carrier in terms of the fractal renewal point process by using the definition of $q(E)$ given above and Eq. (7.26) (Lowen & Teich, 1992b; Lowen, 1992).

**7.10.3.** Given the conditional mean $q(E)$, each trap is assumed to hold carriers for times that follow an exponential density function:

$$p_\tau\big[t|q(E)\big] = \frac{1}{q(E)}\, e^{-t/q(E)}. \tag{7.27}$$

Average the density provided in Eq. (7.27) over all possible values of $q(E)$ to determine the unconditional trapping-time density. Obtain an asymptotic form for the case $A \ll t \ll B$.